Int J Adv Manuf Technol (2016) 84:705–716
DOI 10.1007/s00170-015-7734-6

ORIGINAL ARTICLE

Effect of torch position and angle on welding quality and welding process stability in Pulse on Pulse MIG welding–brazing of aluminum alloy to stainless steel

Jianxiong Li[1] · **Huan Li**[1] · **Huiliang Wei**[1] · **Ying Gao**[2]

Received: 22 May 2015 / Accepted: 18 August 2015 / Published online: 2 September 2015

Abstract In this paper, Pulse on Pulse metal inert gas (MIG) welding–brazing of 6061 aluminum alloy to 304 stainless steel in a lap configuration was developed to investigate the effect of torch position and angle on the welding quality and welding process stability. Images of arc, electrical signals of welding current, and welding voltage were acquired in synchronous modes by a high-speed camera and electrical signal acquisition system, respectively. The obtained results demonstrate that arc shape, macrostructure, microstructure, and mechanical properties are sensitive to torch aiming position when torch travel angle is 20° and work angle is 0°. However, when travel angle is 20° and work angle is 20°, the effect of torch aiming position is insignificant. It is easier to strike arc and maintain it on the surface of aluminum alloy compared to stainless steel. High-strength joints, whose fracture occurred at heat-affected zones of Al alloys at 89 MPa up to 72 % of the tensile strength of Al alloys, have been obtained. Moreover, a comprehensive evaluation method for the welding process stability based on statistical techniques has been proposed. This method can be easily and quickly integrated in real-time control of the welding process, which provides a quantitative guidance in MIG welding–brazing of aluminum alloy to stainless steel.

✉ Huiliang Wei
weihuiliang@tju.edu.cn

[1] Tianjin Key Laboratory of Advanced Joining Technology, School of Materials Science and Engineering, Tianjin University, Tianjin 300072, China

[2] Tianjin Key Laboratory of High Speed Cutting and Precision Machining, Tianjin University of Technology and Education, Tianjin 300222, China

Keywords Pulse on Pulse MIG welding–brazing · Aluminum alloy · Stainless steel · Torch position and angle · Welding quality · Welding process stability

1 Introduction

In recent years, dissimilar metal joining of light alloys and hard alloys is employed in the industry in order to satisfy the weight reducing and strength enhancing requirement [1–3]. Joining of aluminum alloys (Al alloys) and stainless steel (SS) is typically applied in automotive industry. Conventional fusion welding is undesirable due to the low solubility of iron in aluminum, large difference in physical and chemical properties, and excessive formation of brittle intermetallic compounds. As a result, some advanced welding approaches between Al alloys and SS have been developed by researchers, such as laser welding–brazing [4, 5], friction bonding [6, 7], friction stir welding [8], diffusion bonding [9, 10], brazing [11], and transient liquid phase welding [12]. However, some of these methods need rather high pressure or costly equipment [4–8, 11, 12], and some others could not guarantee the joint mechanical property for the generation of excessive brittle intermetallic compounds [6–10, 12]. Therefore, a high-efficiency and low-cost joining method still remains a target for joining aluminum and steel in promoting the use of hybrid structures [13].

In this work, dissimilar aluminum alloy/stainless steel lap joints were made successfully by Pulse on Pulse metal inert gas (MIG) welding–brazing process, and the effects of torch position and angle on welding quality and welding process stability were studied. Since the research of MIG welding–brazing of aluminum to steel is mainly focused on the macrostructure, microstructure, and mechanical properties of joints, the investigation of welding process stability is fairly rare. In

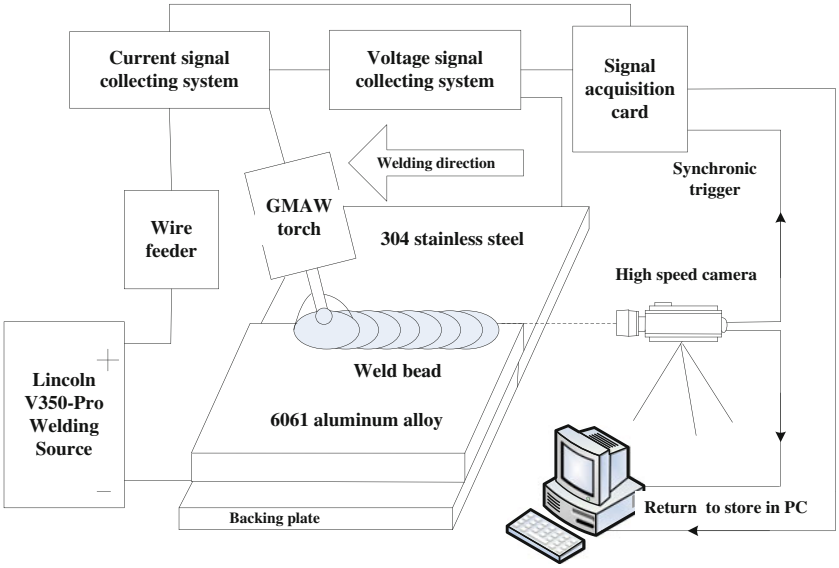

Fig. 1 Schematic illustration of Pulse on Pulse MIG welding–brazing systems

this paper, a comprehensive analysis method based on statistic techniques such as cyclogram (*U-I* characteristic whose welding voltage is a function of welding current intensity) [14, 15], variance of welding voltage [16], and probability density distribution of welding voltage [15] has been proposed to evaluate the welding process stability in welding–brazing of Al alloys to SS.

2 Experimental arrangement

The experimental materials used in this paper are 6061 aluminum alloy (200×60×3 mm) and 304 stainless steel (200×60×2 mm). A 1.2-mm-diameter 4043 Al-Si welding wire was used as the filler metal, and the brazing flux (Al-Powder, Al-Flux, glycol, and anti-precipitation additive) with melt point of 500~650 °C was selected. Argon with a purity of 99.99 % was used as shielding gas.

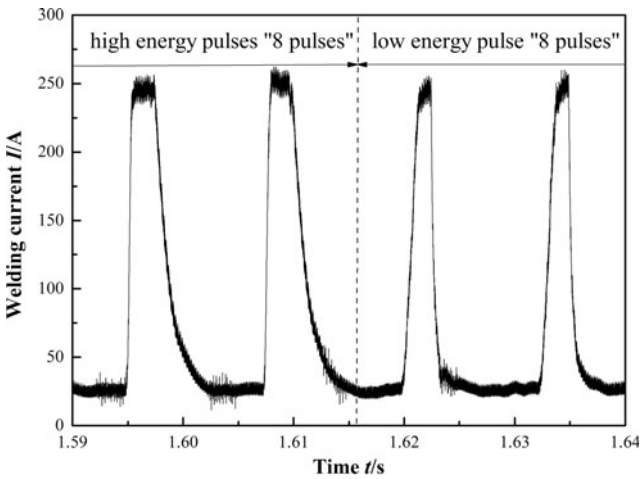

Fig. 2 Schematic diagram of output pulse waveform under Pulse on Pulse mode

Lincoln INVERTEC™V350-PRO was used as welding power source. A high-speed camera (PHOTRON FASTCAM Super 10KC) with capture rate of 1000 frames per second was applied to capture images of arc. An electrical signal acquisition system with maximum sampling frequency of 500 kHz was used to collect electrical signals of welding current and welding voltage. After welding, SEM tests and tensile shear tests were performed as an observation of macrostructure, microstructure, and mechanical property of lap joints of Al alloys to SS.

The schematic illustration of experimental system is shown in Fig. 1. A lap joint configuration is selected because of its application in the auto industry [17]. A direct current with a positively charged electrode (DCEP) current was applied under Pulse on Pulse modes whose output waveform is shown in Fig. 2. In Pulse on Pulse modes, two distinct pulse types are used. A number of high-energy pulses are used to transfer metal across the arc. After a number “8” of such pulses, an identical number “8” of low-energy pulses are performed. These low-energy pulses, shown in Fig. 2, do not transfer any filler metal across the arc and help to cool the arc and

Table 1 Parameters of Pulse on Pulse

Pulse type	Peak current (A)	Background current (A)	Period	Duty cycle (%)
High-energy pulse	270	25	0.0125 s	25
Low-energy pulse	270	25	0.0125 s	17

Table 2 Experimental parameters in MIG welding–brazing

Welding speed	Wire feed rate	Wire extension	Gas flow rate
3 mm/s	3.2 m/min	15 mm	15 L/min

Table 4 Chemical compositions of 304 SS (wt%)

Material	C	Mn	Cr	Si	P	S	Ni	Fe
304 SS	0.08	2.00	18.0~20.0	1.00	0.045	0.03	8.0~11.0	Balance

keep heat input low. The peak current, background current, and frequency are identical for the high-energy and low-energy pulses and are shown in Table 1. The main experimental parameters are given in Table 2. The chemical compositions of 6061 Al alloys, 304 SS, and 4043 Al-Si filler wire are listed in Tables 3, 4, and 5, respectively. The physical properties of 6061 Al alloys and 304 SS are displayed in Table 6.

3 Experimental results and discussion

3.1 The effects of torch position and angle on arc shape and arc stability

The welding–brazing lap joints are obtained by melting the aluminum alloy and forming a connection with SS in solid state through wetting and interfacial reaction. Accordingly, precise control of heat distribution is the key factor to achieve high-quality welds. The varying of torch position and angle results in changing of arc shape, which affects the distribution of heat on sides of Al alloy and SS. The schematic graph of torch position and angle is shown in Fig. 3, where L is torch aiming position, α is the torch travel angle, and β is the work angle. The minus sign means that arc acts at Al alloys sheet.

The effect of torch position and angle on averaged welding resistance for the case shown in Fig. 4 was studied. The average welding resistance is the average of the sum of ratio of the instantaneous welding voltage and welding current acquired by electrical signals acquisition system. The correlation between averaged welding resistance and torch position and angle was elucidated in Fig. 4.

As shown in Fig. 4, when α is 20° and β is 0°, the average welding resistance increases slightly with L increasing from −2 to 1 mm and rises dramatically when L increases from 1 to 2 mm. This dramatic increase can be explained by the differences in melting point, work function, and ionization voltage of Al alloys and SS shown in Tables 6 and 7. As presented, the melting point, work function, and ionization voltage of Al are lower than those of Fe, Cr, and Ni mainly existed in the metal vapor of SS, indicating that Al is more easily vaporized and ionized and that the electron is easier to emit from the surface of Al than SS. Hence, when the torch moves from aluminum alloys to stainless steel side, the current density is decreased, the ionization degree of arc mainly constituted by argon gas and wire vapor is reduced, and its resistance is increased. Particularly, when L is 2 mm, the arc almost all aims at the SS and the average welding resistance increases rapidly. However, when α and β are both 20°, the average welding resistance does not vary significantly because arc action range changes slightly when torch inclines.

The high-speed images of arc of high-energy pulse in welding–brazing of Al alloy to SS are shown in Fig. 5, which also depicts the relative position of filler wire, arc, Al alloy, and SS.

Arc shape with α of 20° and β of 0° was given in Fig. 6. When L ranges from −2 to 1 mm, arc almost all acts on the aluminum alloys for base current stage; this can probably be ascribed to the differences in work function and ionization voltage of Al alloy and SS as analyzed above.

In Fig. 6, since welding current is in DCEP mode, cathode spots are very unstable that the arc does not root in a fixed position but automatically and constantly look for new oxide film to break down, and then a new cathode spot was generated continuously on the oxide layer owing to minimum voltage principle. When L is −2 mm, arc shape undergoes slight changes at the moment of welding current changing from base to peak stage. However, when L is −1, 0, and 1 mm, arc shape experiences dramatic changes, and the arc is stable for peak welding current stage because of strong stiffness of arc. When L is −2, −1, 0, and 1 mm, arc all acts on the Al alloy sheet for base current stage, but when L is 2 mm, arc strikes on SS sheet at the whole period of welding current because arc is easier to form a conductive path maintaining the least energy consumption at SS sheet in this case.

As presented in Fig. 7, arc shape experiences slight changes with the variation of torch aiming position when the torch inclination angle keeps constant. At the base current stage, arc all strikes on Al alloy sheet resulting in better controllability of

Table 3 Chemical compositions of 6061 Al alloys (wt%)

Material	Cu	Mn	Mg	Zn	Cr	Ti	Si	Fe	Al
6061 Al alloys	0.15~0.4	0.15	0.8~1.2	0.25	0.04~0.35	0.15	0.4~0.8	0.7	Balance

Table 5 Chemical compositions of filler wire (wt%)

Material	Cu	Mg	Zn	Ti	Si	Fe	Al
Filler wire	≤0.3	≤0.05	≤0.1	≤0.2	4.5~6.0	≤0.8	Balance

heat distribution in welding process. At the peak current stage, arc distributes on both sides of Al alloy and SS.

3.2 The effects of torch position and angle on macrostructure

In this part, the effects of torch position and angle on macrostructure were discussed. As presented in preliminary discussion, torch position and angle have a significant influence on arc shape and arc stability, which leads to different weld formations. The weld appearance and macroscopic morphology with different torch aiming positions when α is 20° and β is 0° are shown in Figs. 8 and 9, respectively.

As shown in Fig. 8, different torch aiming positions result in different weld appearances. In particular, weld width ratio of SS side to Al alloys side is sensitive to torch aiming position, which indicates that heat distribution between Al alloy and SS depends on torch aiming position. When L is −2 mm, the ratio is 0.22 and wetting angle is 105°. Liquid filler metal does not sufficiently spread, which causes undercut and large weld reinforcement. The effects of torch aiming position on weld width ratio of SS side to Al alloys side are shown in Fig. 10. According to Figs. 9 and 10, the ratio increases and the wetting angle decreases when L varies from −2 to 2 mm. The greater ratio reveals that molten metal distributes more on SS side. The smaller angle indicates that liquid molten metal spreads more sufficiently. Weld forming is better when L is 1 mm by observing the weld appearance, weld width distribution, and wetting angle.

In Figs. 11 and 12, it can be observed that weld width distribution and wetting angle do not vary significantly even though the torch aiming position changes when α is 20° and β is 20°. This can be ascribed to the effect of plasma flow force formed by axial thrust of electromagnetic pinch force, which determines the droplet transfer path and to some extent mitigates the influence of torch aiming position. However, when the work angle is 0°, the plasma flow force generated by axial thrust is perpendicular to workpiece surface, which has not mitigated the effect of torch aiming position.

3.3 The effects of torch position and angle on mechanical properties and interface layers of joints

In order to investigate mechanical properties of joints, tensile shear tests were conducted. Every specimen is in dimension of 100×12 mm cut by linear cutting machine. All tests were carried out at room temperature using DDL300 tensile testing machine operating with a speed of 0.5 mm/min. The tensile shear tests' results are given in Table 8.

As presented in Table 8, the fracture of specimen 1 occurred at the interface layer with shear strength of 58.2 MPa. Considering about the arc shape in Fig. 6a and weld appearance in Fig. 8a, it can be concluded that joints with sound mechanical property cannot be obtained in this case. In the case of specimens 2, 3, and 4, the maximum force joints can bear all excess 5 kN, and the fracture of specimen 2 occurred at interface layer which is the weakest zone of welded–brazed joint. But, the joint of specimens 3 and 4 whose fracture occurred at heat-affected zones (HAZs) of Al alloy at 89 MPa up to 72 % of the tensile strength of Al alloys. Fracture of specimen 5 occurred at weld depression whose strength is lower than that of other places of joint. For specimens 6 and 7, the fracture locations are at the fusion zone, implying that the strength of interface layer is larger than that of seam. However, fracture of specimen 8 occurred at interface layer, and the maximum force that joint can bear is just 2.673 kN which is significantly lower than in other situations. This phenomenon can be supported by the wavy interface layers whose intermetallic metal compounds (IMC) have a large thickness and tend to grow perpendicularly into the Al alloys as shown in Fig. 13c.

In Fig. 13, the interface layers of welding–brazing joints with different torch aiming positions when α is 20° and β is 20° are demonstrated. It can be clarified that the key factor to realize high-quality joining between Al alloy and SS is to guarantee Al alloy melting but SS in solid state and make filler metal sufficiently wet and spread, which can help result in reliable connection with SS through interfacial reaction.

Table 6 Mechanical properties of 6061Al alloys and 304SS

Base metal	Tensile strength (MPa)	Elongation (%)	Melting point (°C)	Density (g/cm^3)	Linear expansion coefficient (10^{-6} K^{-1})	Thermal conductivity (W m^{-1} K^{-1})	Electrical resistivity (10^{-6} Ω·m)
6061Al alloys	124	25	580~650	2.73	23.6	167	0.04
304 SS	≥500	≥40	1398~1454	7.93	18.4	21.5	0.73

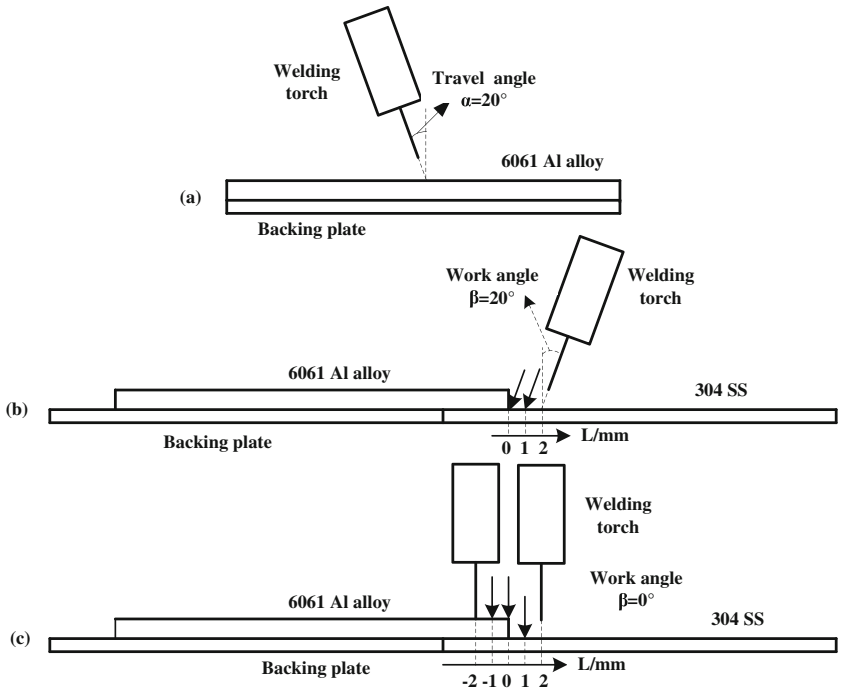

Fig. 3 The schematic graph of torch position and angle. α=20°, β=0° or 20° (**a**). α=20°, β=20° with L varying from 0 to 2 mm (**b**) and α=20°, β=0° with L varying from −2 to 2 mm (**c**)

3.4 Evaluation for the welding process stability of Pulse on Pulse welding–brazing of Al alloy to SS based on analysis of welding electrical signals

To solve the problem of poor welding process stability in Pulse on Pulse MIG welding–brazing of aluminum alloys to stainless steel, this paper proposes a method of determining the welding process stability based on a comprehensive assessment of voltage−current cyclogram (welding voltage as a function of welding current), variance of welding voltage, and probability density distribution.

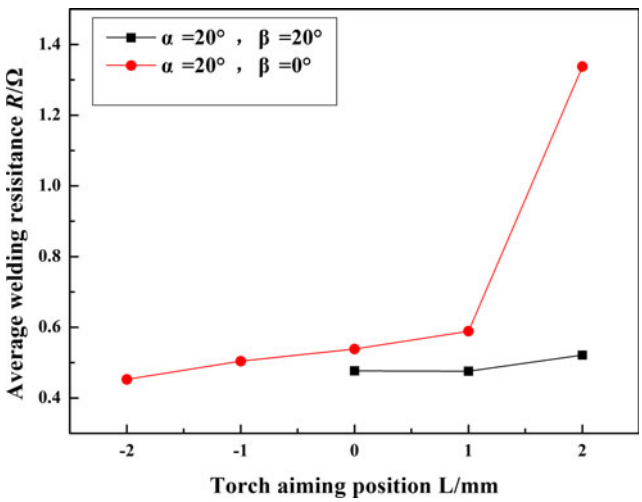

Fig. 4 The average welding resistance with different torch position and angle

As discussed in [15], cyclograms are dynamic movement of operating points which show the welding voltage as a function of the welding current intensity. Cyclograms are a very uncomplicated and fast presentation as far as the welding process stability is concerned. Voltage−current characteristic may be noticed in the cyclogram. In previous studies, a greater stability is observed when *U-I* characteristic occupies a smaller area.

Contrary to preliminary research, this work proposes a method of determining the welding process stability based on the concentration of tracks of *U-I* dynamic operating points. The concentration of tracks of *U-I* dynamic operating points is represented by the area of *U-I* characteristic, which is quantitatively computed by MATLAB software. The smaller the area of *U-I* characteristic, the more concentrated the *U-I* operating points' tracks, and the more stable the welding process will be; otherwise, the lager the area of *U-I* characteristic,

Table 7 The work function and ionization voltage of different elements

Element	Al	Fe	Cr	Ni
Work function (eV)	4.28	4.5	4.5	4.3
Ionization voltage (V)	5.99	7.87	6.77	7.64

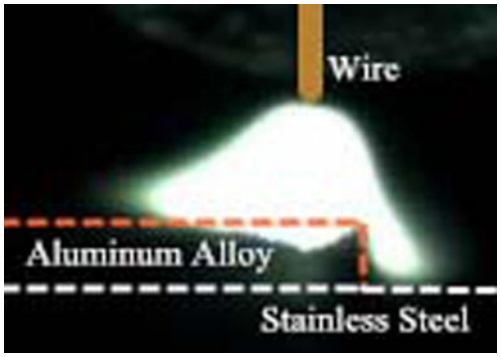

Fig. 5 Shape of arc of high energy pulse

the more dispersed the *U-I* operating point track, and the more unstable the welding process will be.

The theory of cubic spline interpolation function is introduced to compute the occupied area of *U-I* characteristic in MATLAB. In mathematics, the definition of cubic spline interpolation function is expressed as follows: assuming that there are $n+1$ points in $\{(x_k,y_k)\}_{k=0}^{n}$ under condition of $x_0<x_1<\cdots<x_n$. If there are n cubic polynomials, their coefficients are $S_{k,0}$, $S_{k,1}$, $S_{k,2}$, and $S_{k,3}$, simultaneously satisfying the following properties [18]:

$$S(x)=S_k(x)=S_{k,0}+S_{k,1}(x-x_k)+S_{k,2}(x-x_k)^2+S_{k,3}(x-x_k)^3 \quad x\in[x_k,x_{k+1}],\ \text{and}\ k=0,\ \ 1,\ \ 2\cdots,\ \ \text{n}-1. \tag{1}$$

$$S(x_k)=y_k,\quad k=0,\ \ 1,\cdots,\text{n}. \tag{2}$$

$$S_k(x_{k+1})=S_{k+1}(x_{k+1}),\quad k=0,\ \ 1,\cdots,\text{n}-2. \tag{3}$$

$$S_k'(x_{k+1})=S_{k+1}'(x_{k+1}),\quad k=0,\ \ 1,\cdots,\text{n}-2. \tag{4}$$

$$S_k''(x_{k+1})=S_{k+1}''(x_{k+1}),\quad k=0,\ \ 1,\cdots,\text{n}-2. \tag{5}$$

Therefore $S(x)$ is called cubic spline interpolation function.

Property 1 describes that $S(x)$ must be made up of cubic polynomials; property 2 depicts cubic sectionalized interpolation for a given set of data points; property 3 and property 4 ensure that cubic subsectionalized polynomial is a smooth and continuous function; property 5 guarantees the second derivative of function is continuous.

While cubic spline interpolation function is of good astringency, stability, and second-order smoothness, it must satisfy the condition of $x_0<x_1<\cdots<x_n$. This fact makes it difficult for computing area of boundary graph of cyclograms, whose horizontal ordinates (X) and longitudinal ordinates (Y) cannot fit that condition. In this paper, parameter equation method is used. First, suppose that t is monotonic, that is $t_0<t_1<t_2<\cdots<t_n$, interpolating t and X, and t and Y by exploiting cubic spline interpolation in MATLAB.

Making edge optimization for cyclograms of every parameter in Origin8 software, which chooses working points closest to the boundary edge and abandons those deviated from the focusing zone. The cyclograms and boundary graphs

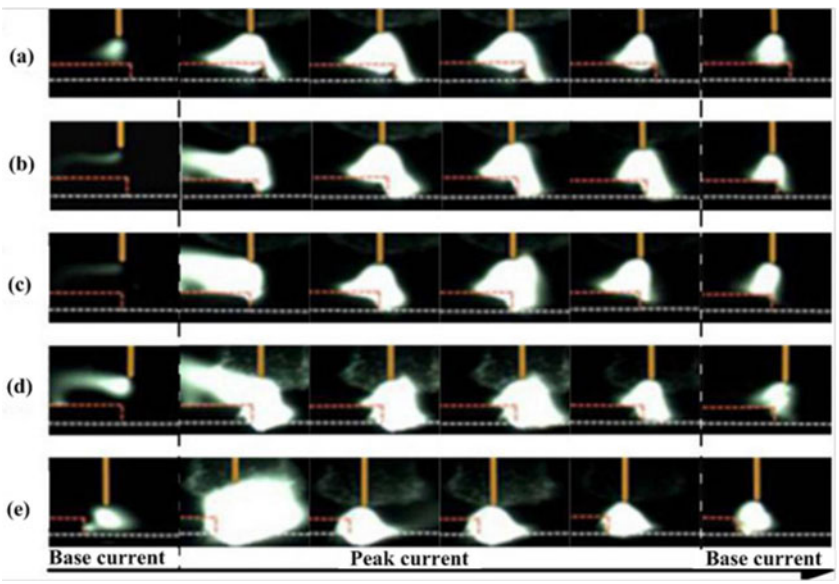

Fig. 6 Arc shape with different torch aiming positions when α is 20° and β is 0°. $L=-2$ mm (**a**), $L=-1$ mm (**b**), $L=0$ mm (**c**), $L=1$ mm (**d**), and $L=2$ mm (**e**)

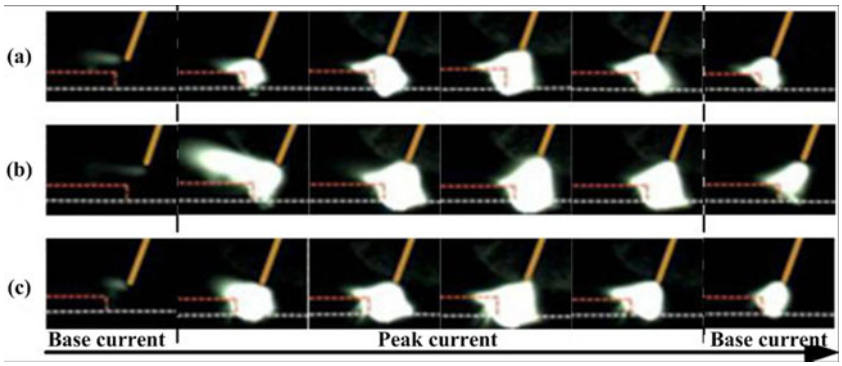

Fig. 7 Arc shape with different torch aiming positions when α is 20° and β is 20°. L=0 mm (**a**), L= 1 mm (**b**), and L=2 mm (**c**)

when L is −1 and 1 mm with α of 20° and β of 0° are shown in Figs. 14 and 15, respectively. The areas when torch aiming position (L) is −1 and 1 mm are represented by S_1 and S_2, respectively.

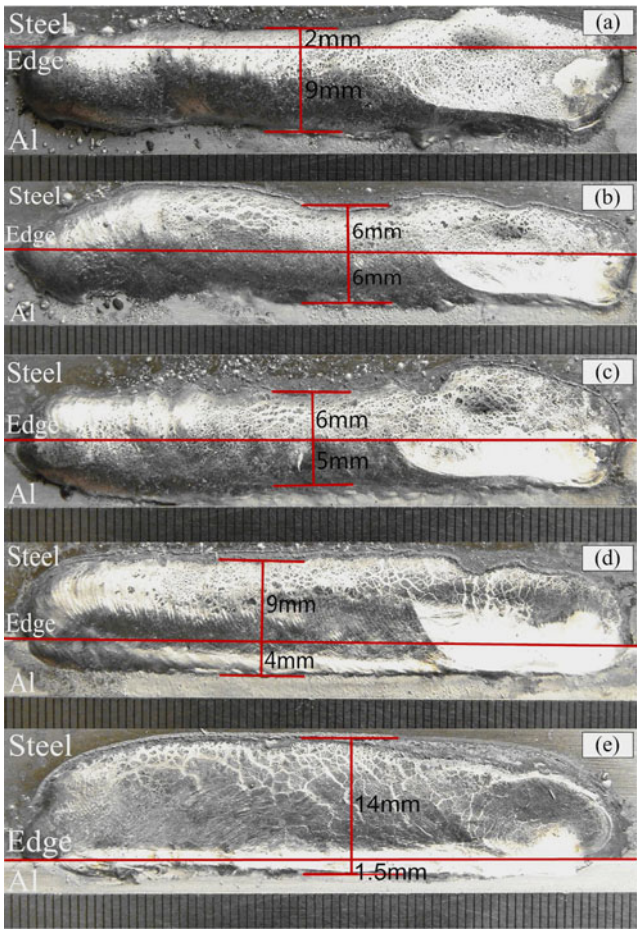

Fig. 8 Weld appearance with different torch aiming positions when α is 20° and β is 0°. L=−2 mm (**a**), L=−1 mm (**b**), L=0 mm (**c**), L=1 mm (**d**), and L=2 mm (**e**)

The cyclograms give the sequential representation of events of arc: The line AB in a typical cyclogram (Figs. 14 and 15) represents the short-circuit stage whose voltage is low and current is high, line BC represents droplet detachment or arc re-ignition whose current is almost constant and voltage is varying at a certain range, line CD represents the arc burning stage whose voltage is high and current is declining fast due to thermal inertia of the arc plasma, and line DA represents wire contact or arc collapse. As shown in Fig. 15a, line BC is more curvy than that in Fig. 14a, indicating that fluctuation of welding current in arc re-ignition stage in Fig. 15 is larger than that in Fig. 14. The line DA in both situations is wider than line BC, noting that fluctuation of welding voltage in arc collapse stage is larger than that in arc re-ignition stage. As presented, the area of cyclogram S_1 is larger than that of S_2, demonstrating that tracks of *U-I* dynamic operating points in Fig. 15 are less concentrated than those in Fig. 14.

However, we cannot make a conclusion that the welding process stability is greater in Fig. 14. Subsequent analyses are clarified to verify the notion that the more concentrated the tracks of *U-I* dynamic operating points, the more stable the welding process.

According to statistics theory, variances of variables can be used to demonstrate the deviation between variables and the mean (average of variables), thereby reflecting the stability of variables. The expression of variance of variables are as follows:

$$\overline{X} = \frac{1}{n}\sum_{i=1}^{n} X_i \tag{6}$$

where $\overline{X}$ is the sample average, n is the sample size, and X_i is the variable value:

$$S^2 = \frac{1}{n-1}\sum_{i=1}^{n}\left(X_i - \overline{X}\right)^2 \tag{7}$$

where S^2 is the sample variance and $\overline{X}$ is the sample average.

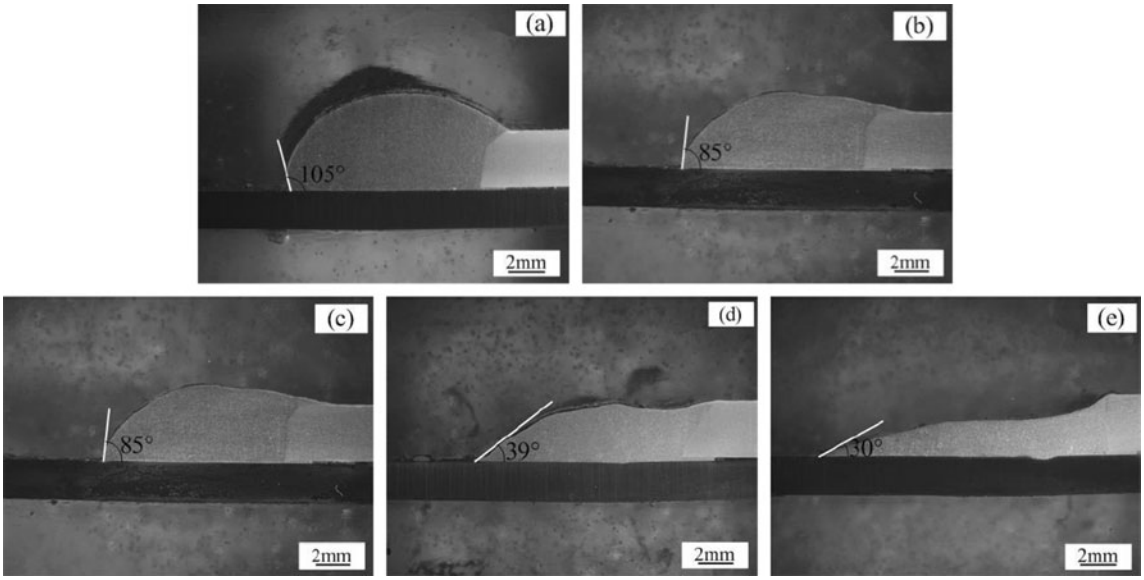

Fig. 9 Macroscopic morphology of joints with different torch aiming positions when α is 20° and β is 0°. L=−2 mm (**a**), L=−1 mm (**b**), L=0 mm (**c**), L=1 mm (**d**), and L=2 mm (**e**)

In the process of MIG welding, the relationship between welding voltage and arc length is expressed in the following equation [19]:

$$U_a = U_c + U_A + EL \tag{8}$$

where U_a is the welding voltage, U_c is the cathode voltage drop, U_A is the anode voltage drop, E is the voltage drop of unit arc length, and L is the arc length.

According to Eq. (8), welding voltage is proportional to the arc length so that the fluctuation of welding voltage represented by its variance reflects the stability of arc, indicating that variance of welding voltage can be an index of welding process stability [20].

The waveform maps of welding voltage in range of 2.2~2.6 s when torch aiming position (L) is −1 and 1 mm with α of 20° and β of 0° are shown in Fig. 16a, b, respectively.

As presented in Fig. 16, fluctuation of waveform of welding voltage in (b) is larger than that in (a), showing as $S_2^2 > S_1^2$, which demonstrates that the stability of welding

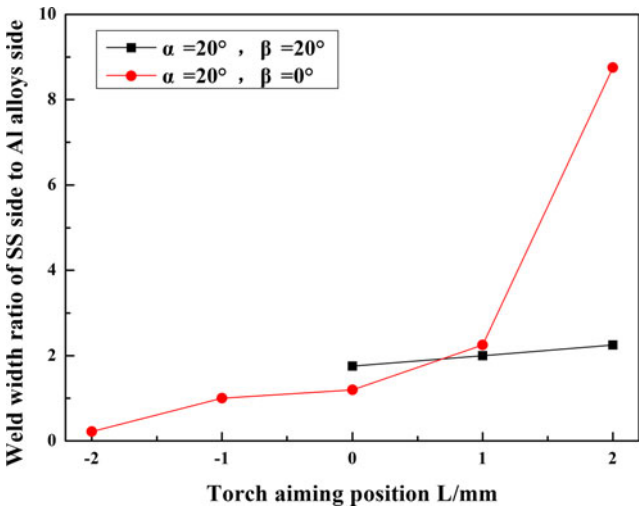

Fig. 10 Weld width ratio of SS side to Al alloys side with different torch aiming positions

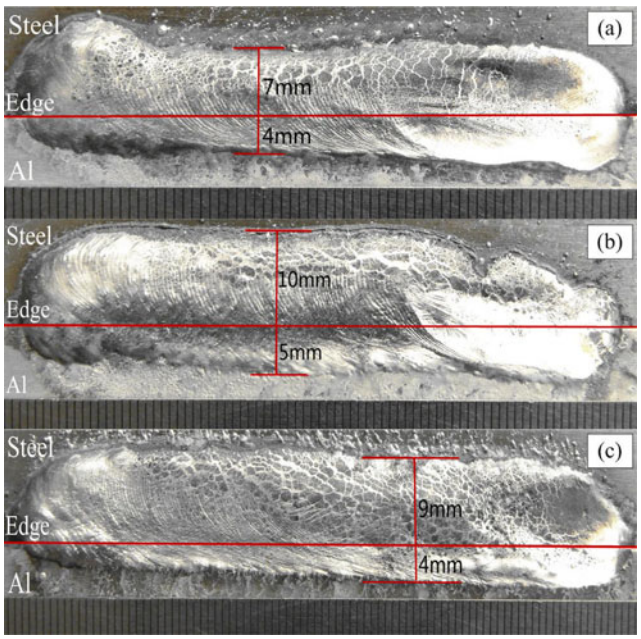

Fig. 11 Weld appearance with different torch aiming positions when α is 20° and β is 20° L=0 mm (**a**), L=1 mm (**b**), and L=2 mm (**c**)

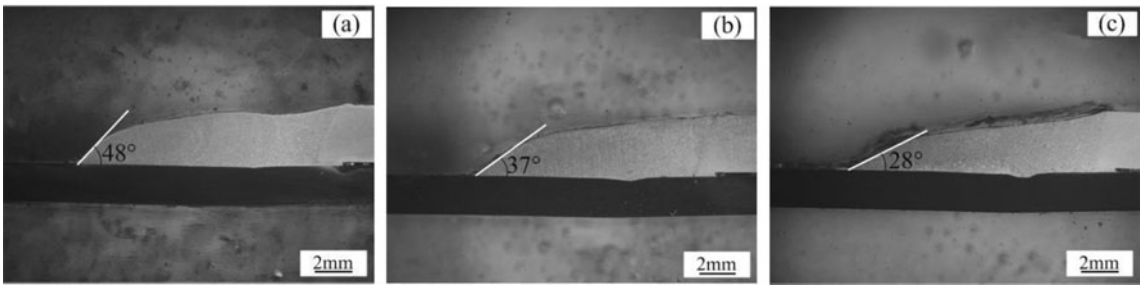

Fig. 12 Macroscopic morphology of joints with different torch aiming positions when α is 20° and β is 20°. L=0 mm (**a**), L=1 mm (**b**), and L=2 mm (**c**)

voltage in (a) is greater than that in (b). So it can be concluded that the arc is more stable in situation (a).

The probability density distribution (PDD) of welding voltage represents proportions in which the welding voltage varies during the welding process. The PDD of welding voltage when L is −1 mm and L is 1 mm with α of 20° and β of 0° are shown in Fig. 17.

The ratio of the peak probability density (PPD) of welding voltage can be an evaluation of welding process stability: The smaller the ratio of the PPD of welding voltage, indicating that the droplet transfer occurred mainly at the peak current stage, the more stable the welding process will be; the greater the ratio of the PPD of welding voltage, indicating the droplet transfer occurred mainly at the base current stage, the more unstable the welding process will be. As displayed in Fig. 17, the ratio of PPD when L is 1 mm is larger than that when L is −1 mm, and in the former case, welding voltage is distributed in range of 35~40 V, indicating that there are abnormal values of welding voltage in this situation which leads to more unstable welding process in comparison with the latter case.

As discussed above all, it can be clarified that analysis of variance and PDD of welding voltage can be a verification to the theory of cyclograms, noting that a greater stability is observed when *U-I* characteristic occupies a smaller area. It can be concluded that area of *U-I* characteristic occupied, variance of welding voltage, and PDD of welding voltage can be a comprehensive estimation of welding process stability of Pulse on Pulse MIG welding–brazing of Al alloys to SS.

4 Conclusions

In Pulse on Pulse MIG welding–brazing of aluminum alloy to stainless steel, torch position and angle have a significant effect on welding quality and welding process stability. The conclusions are listed as follows:

1. Arc shape, macrostructure, microstructure, and mechanical properties are sensitive to torch aiming position when torch travel angle α is 20° and work angle β is 0°. High-strength joints whose fracture occurred at heat-affected zones (HAZs) of Al alloys at 89 MPa up to 72 % of the tensile strength of Al alloy have been obtained with torch aiming position of 0 and 1 mm. However, when α is 20° and β is 20°, the effect of torch aiming position is insignificant. This can be ascribed to the effect of plasma flow force formed by axial thrust of electromagnetic pinch force, which determines the droplet transfer path and to some extent mitigates the influence of torch aiming position.

Table 8 Results of tensile shear tests

Specimen	α (degrees)	β (degrees)	L (mm)	Maximum force (kN)	Fracture location	Thickness of IMC layers (μm)	Tensile shear strength (MPa)
1	20	0	−2	3.491	Interface layer	3.0	58.2
2	20	0	−1	5.277	Interface layer	3.2	88.0
3	20	0	0	5.348	HAZ of Al alloy	2.8	89.1
4	20	0	1	5.349	HAZ of Al alloy	3.3	89.2
5	20	0	2	3.114	Weld depression	4.7	51.9
6	20	20	0	4.885	Fusion zone	1.8	81.4
7	20	20	1	5.222	Fusion zone	2.6	87.0
8	20	20	2	2.673	Interface layer	6.0	44.6

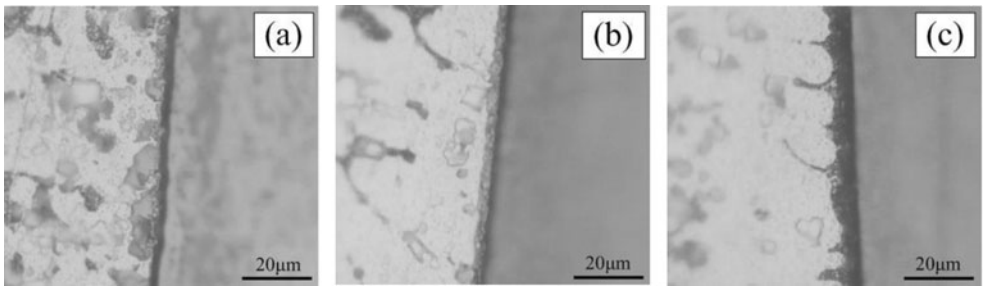

Fig. 13 Interface layer of welding–brazing joints with different torch aiming positions when α is 20° and β is 20°. L= 0 mm (**a**), L=1 mm (**b**), and L= 2 mm (**c**)

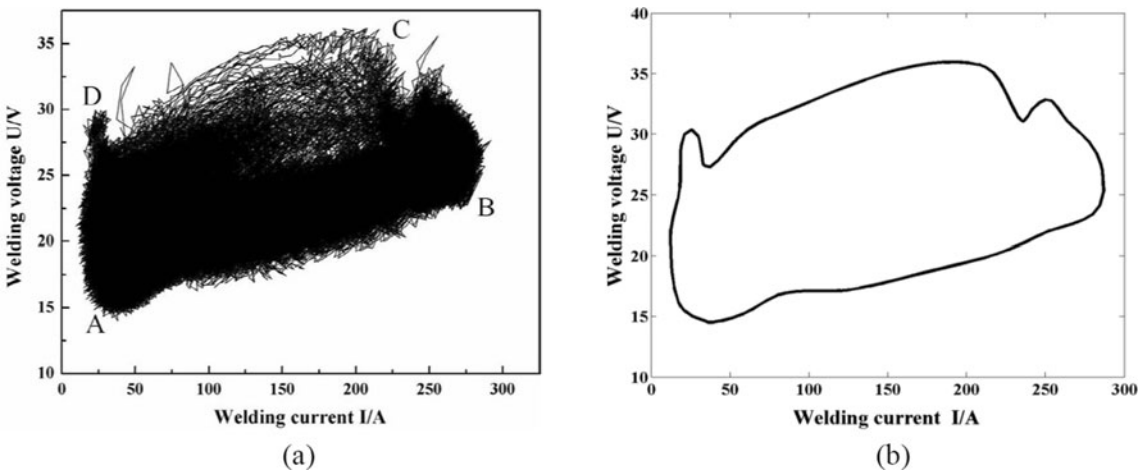

Fig. 14 Cyclogram (**a**) and its boundary map (**b**) when L is −1 mm, S_1=3.3224e+003

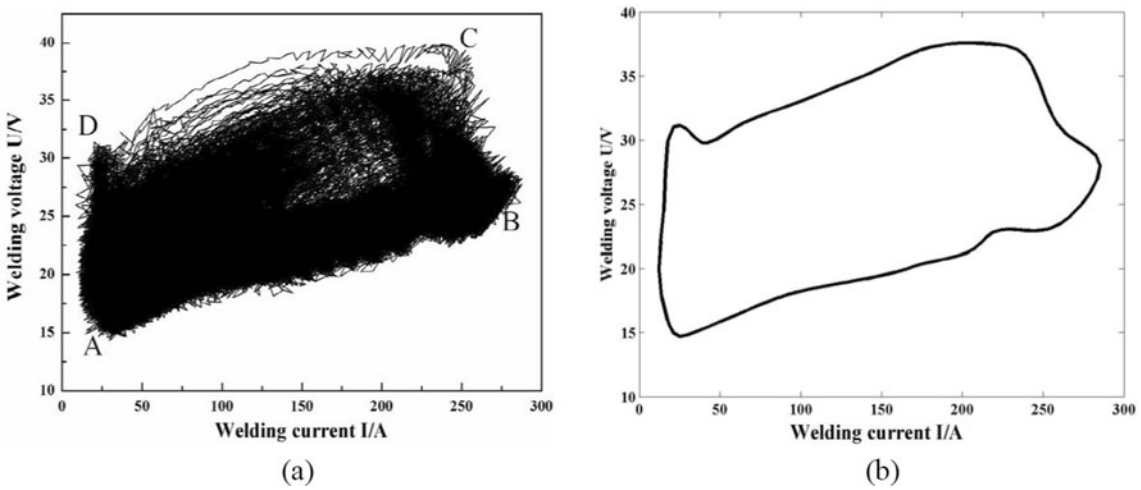

Fig. 15 Cyclogram (**a**) and its boundary map (**b**) when L is 1 mm, S_2=3.8061e+003

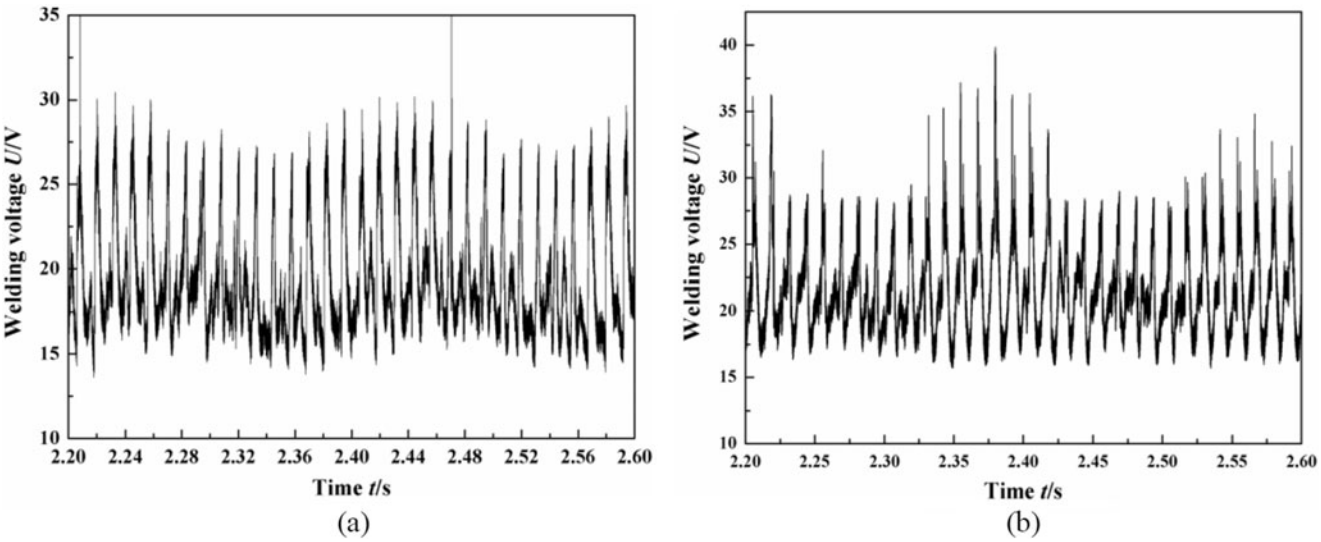

Fig. 16 The waveform maps of welding voltage in range of 2.2~2.6 s when L is −1 mm, S_1^2=10.11 (**a**) and L is 1 mm, S_2^2=11.63 (**b**) with α of 20° and β of 0°

2. The difference of heat distribution on sides of Al alloy and SS is the key factor to the varying of ratio of weld width distribution with different torch aiming positions.
3. It is easier to strike arc and maintain it on the surface of aluminum alloy compared to stainless steel. The oxide films on the surface of aluminum alloy attract the arc and form cathode spot. Arc shape will be affected by changing the torch aiming position with welding current varying from base to peak stage.
4. An evaluation method for welding process stability of Pulse on Pulse welding–brazing of Al alloy to SS based on a comprehensive estimation of cyclograms, variance, and probability density distribution of welding voltage has been proposed. This analysis approach can be easily and quickly integrated in real-time control of the welding process, which provides a quantitative guidance in MIG welding–brazing of aluminum alloy to stainless steel.

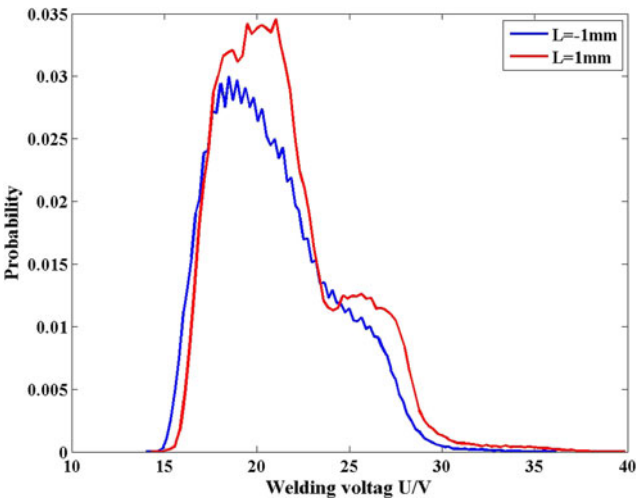

Fig. 17 The PDD of welding voltage when L is −1 and 1 mm with α of 20° and β of 0°

Acknowledgments This work was supported by the National Natural Science Foundation of China (grant no.51475325) and Tianjin Research Program of Application Foundation and Advanced Technology (grant no. 14JCYBJC19100).

References

1. Mahendran G, Balasubramanian V, Senthilvelan T (2009) Developing diffusion bonding windows for joining AZ31B magnesium and copper alloys. Int J Adv Manuf Technol 42:689–695
2. Elthalabawy WM, Khan TI (2011) Eutectic bonding of austenitic stainless steel 316L to magnesium alloy AZ31 using copper interlayer. Int J Adv Manuf Technol 55:235–241
3. Chen YB, Chen SH, Li LQ (2009) The effect of heat input on microstructure and mechanical property of Al/Ti joints by rectangular spot laser welding-brazing method. Int J Adv Manuf Technol 44:265–272
4. Tan CW, Li LQ, Chen YB, Mei CX, Guo W (2013) Interfacial microstructure and fracture behavior of laser welded-brazed Mg alloys to Zn-coated steel. Int J Adv Manuf Technol 68:1179–1188
5. Chen HC, Pinkerton AJ, Li L (2011) Fibre laser welding of dissimilar alloys of Ti-6Al-4V and Inconel 718 for aerospace applications. Int J Adv Manuf Technol 52:977–987
6. Handa A, Chawla V (2014) Investigation of mechanical properties of friction-welded AISI 304 and AISI 1021 dissimilar steels. Int J Adv Manuf Technol 75:1493–1500

7. Arivazhagan N, Singh S, Prakash S, Reddy GM (2008) An assessment of hardness, impact strength and hot corrosion behavior of friction-welded dissimilar weldments between AISI 4140 and AISI 304. Int J Adv Manuf Technol 39:679–689
8. Chen YC, Nakata K (2009) Microstructural characterization and mechanical properties in friction stir welding of aluminum and titanium dissimilar alloys. Mater Des 30:469–474
9. Sohn WH, Bong HH, Hong SH (2003) Microstructure and bonding mechanism of Al/Ti bonded joint using Al–10Si–1Mg filler metal. Mater Sci Eng A 355:231–240
10. Yao W, Wu AP, Zou GS, Ren JL (2008) Formation process of the bonding joint in Ti/Al diffusion bonding. Mater Sci Eng A 480: 456–463
11. Takemoto T, Okamoto I (1988) Intermetallic compounds formed during brazing of titanium with aluminium filler metals. J Mater Sci 23:1301–1308
12. AlHazaa A, Khan TI, Haq I (2010) Transient liquid phase (TLP) bonding of Al7075 to Ti–6Al–4V alloy. Mater Charact 61:312–317
13. Zhang HT, Liu JK (2011) Microstructure characteristics and mechanical property of aluminum alloy/stainless steel lap joints fabricated by MIG welding-brazing process. Mater Sci Eng A 528:6179–6185
14. Suban M, Tušek J (2003) Methods for the determination of arc stability. J Mater Process Technol 143(144):430–437
15. Moinuddin SQ, Sharma A (2015) Arc stability and its impact on weld properties and microstructure in anti-phase synchronised synergic-pulsed twin-wire gas metal arc welding. Mater Des 67: 293–302
16. Niagaj J (2002) An assessment of arc stability during welding with basic shielded electrodes. Weld Int 16:593–598
17. Li X, Lawson S, Zhou Y (2007) Novel technique for laser lap welding of zinc coated sheet steels. J Laser Appl 19:259–264
18. Wu ZY (2010) Scientific computing experiment guide book of numerical analysis based on MATLAB. China University of Geosciences Press 59–60
19. Yang CL, Lin SB (2010) Bases of arc welding. Harbin Institute of Technology Press 36–37
20. Cai XY, Li H, Wei HL, Yang LJ, Gao Y (2014) Effect of laser on the welding process of short-circuiting transfer MIG welding of aluminum alloys. Int J Adv Manuf Technol 75:1829–1836